IET Renewable Power Generation

Research Article

IET Journals
The Institution of Engineering and Technology

Oscillatory stability assessment of microgrid in autonomous operation with uncertainties

ISSN 1752-1416
Received on 31st August 2017
Revised 20th November 2017
Accepted on 11th December 2017
E-First on 1st February 2018
doi: 10.1049/iet-rpg.2017.0579
www.ietdl.org

Awan Uji Krismanto[1,2], Nadarajah Mithulananthan[1] ✉, Innocent Kamwa[3]

[1]*University of Queensland, Brisbane, Australia*
[2]*National Institute of Technology, Malang, Indonesia*
[3]*Hydro-Québec Research Institute (IREQ), Varennes, Canada*
✉ *E-mail: mithulan@itee.uq.edu.au*

Abstract: One of the main challenges of the microgrid (MG) operation in autonomous mode is the uncertain output due to the fluctuating nature of renewable energy resources (RES). This study investigates the effects of RES uncertainties to the oscillatory stability of a hybrid MG in islanded operation. A comprehensive model of Wind Energy Conversion System (WECS), a two-stage Photovoltaic (PV) and bio--diesel engine (BDE) based distributed generation (DG) units are considered to capture a complete dynamic response of the hybrid MG. Trajectories and distribution of damping ratios and oscillatory frequencies of the critical modes were thoroughly investigated through Monte Carlo simulation considering wind speed and solar irradiance uncertainties. From the probabilistic study, it was observed that the presence of RES variations results in a dynamic change of power-sharing strategies and introduce an adverse effect on small signal stability. Uncertain condition of wind speed brings more deterioration in system damping than solar irradiation variation. From time domain simulation, it was confirmed that at higher wind speed, damping on the critical modes reduced. As a consequence, the hybrid MG experienced more oscillatory conditions and even lead to unstable situation at high wind speed conditions. While with solar irradiance change, the investigated MG system can maintain its stable operation.

1 Introduction

Power system operations were continuously subjected to several uncertain conditions such as random change of load profile and adjustment of dispatched power generation. These uncertainties cause a change in equilibrium points of power system operation. In transition stages, change of operating point results in damped oscillatory condition until new equilibrium points are achieved if sufficient sources are available for damping the critical modes. However, when the system damping was not sufficient to damp the oscillation, a growing oscillatory amplitude emerged and an unstable situation occurred. In a deregulated power system environment with penetration of distributed generation (DG) powered by renewable energy resources (RES), the risk of uncertainties increases in proportion to RES power generation. The stochastic and intermittent characteristics of RES introduce novel challenges in power system stability.

Traditionally, the deterministic modal analysis was performed to investigate small signal stability performance in the power system. However, the deterministic method was not able to capture the variability and stochastic features of RES since only limited scenarios were considered [1–3]. Moreover, it is difficult to assess the risk of instability from the deterministic analysis. These drawbacks encouraged the implementation of a probabilistic approach which fully considers possible uncertainties in analysing small signal stability. Various methods have been proposed to study the effects of uncertainties in power system small signal stability [3–8]. Among the proposed probabilistic analytical methods, Monte Carlo (MC) simulation (MCS) has been a popular method due to its ability to handle a large number of samples with high accuracy and flexibility [1, 4]. In [1, 2, 7, 9–11], the effect of wind energy conversion system (WECS) power uncertainty on the oscillatory condition of the power system was investigated through MCS. It was reported that increased WECS penetration in the existing grid deteriorated system dynamic response and damping performance. The distribution of critical eigenvalues, damping, and oscillatory frequency was presented to quantify the possibility of the unstable situation due to the wind speed variation.

More stability concerns involving small signal stability corresponding to the RES uncertainties emerged in a system with dominant power supplies from RES such as in a microgrid (MG) system. In islanding mode, each DG unit is operated using a certain power-sharing strategy to ensure stable MG operation. As power output from DG units varied due to the RES uncertainties, the power-sharing scheme in the MG changed accordingly which might disturb the power generation and load demand balance. When the generation-load balance is perturbed, the critical eigenvalues deviated significantly, yielding deterioration of the system dynamic response [12, 13]. The balanced situation in the MG can be maintained by providing an accurate power-sharing strategy among DG units which is realised by the proper tuning of the droop gain controller. It was reported from the previous research that the change of droop gain introduced significant effects on the oscillatory stability in the MG [14–17]. Since the RES uncertainties significantly influenced the power-sharing scheme and MG stability, the oscillatory stability analysis of islanding MG operation considering RES uncertainties is crucial to ensure stable supply to the customers within the MG.

Even though the RES uncertainties are a key element in MG stability, only a few works investigated probabilistic small signal stability in autonomous MG. Most of the research presented stability analysis of the MG under variation of the power-sharing scheme in a specific range of droop gain parameters [14, 15, 17–19]. For MG design and planning purposes, it is important to determine the risk of instability under different MG operating points. Therefore, how the RES uncertainties affect the power-sharing scheme and dynamic response of the MG should be carefully investigated. The main concern in observing the uncertainties in the MG is how to incorporate stochastic features of RES into a developed comprehensive model MG in [17, 19], to provide a complete picture of MG dynamic behaviour when it is operated under uncertain operating points. Another concern in presenting statistical analysis from the probabilistic small signal stability study is how to extract the investigated critical modes from a large number of eigenvalue data.

This study addressed the stochastic analysis of oscillatory stability in hybrid MG considering RES uncertainties. A comprehensive model of a hybrid MG consisting of WECS, PV, and bio-diesel engine (BDE)-based DG units as presented in [17, 19] is considered. To take into account the RES uncertainties, the droop control method in the previous MG model should be modified hence it can be adaptively tuned by RES variations. Dynamic MG responses associated with the different power-sharing strategies are thoroughly observed using MCS. Clustering techniques are then applied to extract the critical eigenvalues which dominantly influenced the MG small signal stability performance. Eventually, the statistical properties of the critical eigenvalues are then analysed to determine the oscillatory stability performance and assess the risk of instability.

The remainder of the paper is organised as follows. The estimation procedures of the wind speed and solar irradiance probabilistic models are presented in Section 2. The framework of the proposed MCS method for analysing stochastic oscillatory stability in the MG is presented in Section 3. In Section 4, eigenvalue analysis and clustering techniques for critical mode identification are presented. While the modelling procedures of the hybrid MG system and its modified droop controller are described in section 5. The simulation results are presented and discussed in Section 6. Eventually, conclusions and contributions of this study are highlighted in Section 7.

2 Probabilistic model of RES

The probabilistic distribution functions (PDFs) are estimated from the collected wind speed and solar irradiance data using Weibull and Gaussian mixture distribution functions, respectively. The estimated RES PDFs are then considered to generate random variables for MCS.

2.1 Probabilistic model of wind speed

Optimal mechanical power obtained from a given wind speed is stated by [20]

$$P_{\text{opt}} = 0.5\rho C_{\text{opt}}(\lambda_{\text{opt}}, \beta)A_{\text{r}}v_{\text{w}}^3, \tag{1}$$

where ρ is the air density (kg/m^3), v_{w} is the wind speed (m/s), A_{r} is the effective area covered by turbine blades in (m^2) and C_{opt} is the optimal power coefficient of a wind turbine for a certain wind speed. While λ_{opt} and β, respectively, represent tip speed ratio and blade pitch angle in degree.

The uncertain condition or random variation of wind speed is represented by a particular PDF. The obtained wind speed data are fitted to the Weibull distribution function. The Weibull probabilistic $f(v)$ and cumulative $F(v)$ distribution functions for a given wind speed are provided as follows:

$$f(v) = \frac{k}{c}\left(\frac{v_{\text{w}}}{c}\right)^{k-1}\exp\left[-\left(\frac{v_{\text{w}}}{c}\right)^{k}\right], \tag{2}$$

$$F(v) = 1 - \exp\left[-\left(\frac{v_{\text{w}}}{c}\right)^{k}\right], \tag{3}$$

where k and c are related to shape and scale parameters of the Weibull distribution function.

The Weibull parameters can be determined through graphical and numerical methods. As presented in [21, 22], among several estimation techniques, the maximum likelihood method provides better accuracy in determining the Weibull parameters as given by the following equations:

$$k = \left[\frac{\sum_{i=1}^{n} v_i^k \ln(v_i)}{\sum_{i=1}^{n} v_i^k} - \frac{\sum_{i=1}^{n}\ln(v_i)}{n}\right]^{-1}, \tag{4}$$

$$c = \left(\frac{1}{n}\sum_{i=1}^{n} v_i^k\right)^{1/k}, \tag{5}$$

where n is the number of observations performed.

For a typical WECS- based DG, the power output can be determined by applying the wind speed data series to (1).

2.2 Probabilistic model of solar irradiance

The PV array consists of PV modules which are installed in series and parallel combination to generate the desired current and output voltage. In this study, an ideal diode model of the PV array is considered [23]. The connection between the PV current and voltage is dictated by

$$I_{\text{pv}} = N_{\text{p}}I_{\text{sc}}\left(\frac{G}{G_{\text{ref}}}\right) - N_{\text{p}}I_{\text{s}}\left[\text{e}^{(qV_{\text{pv}}/nkTN_{\text{s}})} - 1\right]. \tag{6}$$

To simplify (6), −1 in the last term can be neglected as it is much smaller than the exponential part. The terminal voltage of the PV array is represented as V_{pv}. I_{pv} is the PV current calculated from the short circuit (I_{sc}) and diode saturation (I_{s}) current. N_{p} and N_{s} constitute parallel and series PV modules connections, respectively. T is absolute temperature (K) in PV modules. k dictates Boltzmann (J/K) constant. While q represents charge of the electron (C), n is the ideality factor of the diode. Instantaneous and reference values of solar irradiance are presented by G and G_{ref}, respectively.

The PV array output power is calculated from the product of current and terminal voltage as given by

$$P_{\text{pv}} = V_{\text{pv}}\left\{N_{\text{p}}I_{\text{sc}}\left(\frac{G}{G_{\text{ref}}}\right) - N_{\text{p}}I_{\text{s}}\text{e}^{(qV_{\text{pv}}/nkTN_{\text{s}})}\right\}. \tag{7}$$

The random variation of solar irradiance can be presented in the statistical form using an appropriate PDF. Bimodal density function was developed in [24, 25] to estimate the distribution of hourly measured solar irradiance data. It was found that the PDF of solar irradiance was determined as a function of clearness index using a mathematical model related to Boltzmann statistics. In [26, 27], the generalised approach was considered in calculating density function of solar irradiance. Since the presence of two maxima was monitored without significant variations within a particular range, a Gaussian mixture model was implemented to estimate the solar irradiance PDF. The mixture of two normal Gaussian distribution functions is given by

$$f(G_t) = \tau f_1(G_t) + (1-\tau)f_2(G_t), \tag{8}$$

where f_1 and f_2 are Gaussian density functions of random variables given by

$$f_i = \frac{1}{\sqrt{2\pi\sigma_i^2}}\exp\left[\frac{-0.5(G_t-\mu_i)^2}{\sigma_i^2}\right], \quad i = 1, 2, \tag{9}$$

where τ is the weight of the mixture constant which varied in a specified range of $0 < \tau < 1$. μ_i and σ_i represent the mean and standard deviation of the corresponding density functions of normal random variables.

The parameters of a mixture function popularly determined through the expectation maximisation (EM) method which is similar to the maximum likelihood estimation problem for Gaussians. The EM method is comprised of two steps: an expectation step and a maximisation step which iteratively computes the expectations and applying maximum likelihood for the latent variables, respectively. The parameters of the normal distribution function are updated and determined using the following equations:

$$\tau_i = \frac{1}{N}\sum_{t=1}^{N} G_k^{(t)}, \tag{10}$$

$$\mu_i = \frac{1}{\sum_{t=1}^{N} G_k^{(j)}} \sum_{t=1}^{N} G_k^{(t)} x^{(t)}, \tag{11}$$

$$\sigma_i = \frac{1}{\sum_{t=1}^{N} G_k^{(j)}} \sum_{t=1}^{N} G_k^{(t)} \left(x^{(t)} - \mu_k\right)^2, \tag{12}$$

where $N = 1, 2, \ldots, t$ is the number of samplings.

3 MCS for small signal stability analysis

In uncertainty analysis, the relationship between the dependent and independent variables can be stated as [1, 4]

$$\boldsymbol{v} = h(\boldsymbol{z}), \tag{13}$$

where h represents the function that describes the correlations between the dynamic behaviour of output variables and uncertain values of input variables. The input and output vector variables can be represented as $\boldsymbol{v} = [v_1 \quad v_2 \quad \ldots]^{\mathrm{T}}$ and $\boldsymbol{z} = [z \quad z_2 \quad \ldots]^{\mathrm{T}}$, respectively.

The purpose of uncertainty analysis is to estimate the uncertainty of output or dependent variables that result from uncertainty in the input or independent variables through the particular complex functions. In correlation with the probabilistic analysis, the stochastic study based on the uncertain condition of input variables aim to determine the PDFs of the output variables. To obtain the PDFs of the output variables, the input variables are randomly sampled through an iterative method such as MCS. The main steps of implementing the MC method to investigate small signal stability are as follows:

- Set a number of MC iterations based on the determined sample size of input and output variables.
- Generate random RES values based on their estimated PDFs. Subsequently, the generated random numbers are fed into the detailed hybrid MG model for the modal analysis purpose.
- Iteratively, carry out modal analysis and store the eigenvalue results.
- From a set of obtained eigenvalues, the clustering technique is then conducted to extract the critical modes corresponding to the investigated eigenvalues.
- Eventually, the system damping and dynamic responses were assessed statistically to determine the risk of instability and small signal stability performance.

4 Eigenvalue analysis and clustering

The dynamic stability of a power system can be presented by a set of ordinary differential-algebraic equations as given by the following equations:

$$\begin{aligned} \dot{\boldsymbol{x}} &= \boldsymbol{f}(\boldsymbol{x}, \boldsymbol{u}), \\ \boldsymbol{y} &= \boldsymbol{g}(\boldsymbol{x}, \boldsymbol{u}), \end{aligned} \tag{14}$$

where $\boldsymbol{x} = [x_1 \quad x_2 \quad x_n]^{\mathrm{T}}$ is the vector of state variables, $\boldsymbol{y} = [y_1 \quad y_2 \quad y_n]^{\mathrm{T}}$ is the vector of system output variables, $\boldsymbol{u} = [u_1 \quad u_2 \quad u_n]^{\mathrm{T}}$ is the vector of system input variables. While non-linear functions which define state and output variables are presented as $\boldsymbol{f} = [f_1 \quad f_2 \quad f_n]^{\mathrm{T}}$ and $\boldsymbol{g} = [g_1 \quad g_2 \quad g_n]^{\mathrm{T}}$, respectively.

The modal analysis which describes the dynamic behaviour of the system when it is exposed to the small disturbances is derived from the linearisation of (14) around a certain operating point. The linearised equation can be represented by a set of state space equations as given by the following equation:

$$\begin{aligned} \boldsymbol{\Delta}\dot{\boldsymbol{x}} &= \boldsymbol{A}\boldsymbol{\Delta}\boldsymbol{x} + \boldsymbol{B}\boldsymbol{\Delta}\boldsymbol{u}, \\ \boldsymbol{\Delta}\boldsymbol{y} &= \boldsymbol{C}\boldsymbol{\Delta}\boldsymbol{x} + \boldsymbol{D}\boldsymbol{\Delta}\boldsymbol{u}, \end{aligned} \tag{15}$$

where prefix Δ denotes a small deviation of the corresponded state variables. $\boldsymbol{\Delta x}$ and $\boldsymbol{\Delta} y$ represent state vector and output vector variables, respectively. While $\boldsymbol{\Delta u}$ represents the input vector variables. State, input, and output matrices are defined as $\boldsymbol{A}$, $\boldsymbol{B}$ and $\boldsymbol{C}$, respectively. The matrix $\boldsymbol{D}$ describes the connection between input and output variables.

Important information related to the oscillatory condition and system dynamic response is derived from the eigenvalues of state matrix $\boldsymbol{A}$.The critical modes are characterised by the damping ratio (ζ) which denotes the rate of decay or increasing amplitude of oscillation corresponding to the stable and unstable situation, respectively. The oscillatory stability circumstances can be categorised into three regions: stable condition corresponding to a well-damped situation with a damping ratio >5% ($\zeta \geq 5\%$), critically stable associated with more oscillatory conditions with a damping ratio in the range of 0–5% ($0\% \leq \zeta \leq 5\%$) and the unstable region with a negative damping ratio ($\zeta < 0\%$), indicated undamped condition with continuously increased oscillatory magnitude.

The characterisation of critical eigenvalues can be conducted by investigating the contribution of the state variables in their particular modes. The participation factor provides worthy information regarding the relationship between the states and modes [28]. Higher participation factor values show more relevant state variables to the modes. The participation factor of ith state variables and kth modes is given by

$$p_{ik} = \phi_{ik}\psi_{ik}, \tag{16}$$

where ϕ_{ik} and ψ_{ik}, respectively, represent the element on the right eigenvector and left eigenvector.

Conventionally, participation factor analysis was conducted to identify the unstable eigenvalues based on contributions of state variables in the corresponding modes. However, in probabilistic small signal stability analysis with a significant number data, the participation factor approach should be combined with the clustering method to extract the sensitive modes from a large number of obtained eigenvalues. A clustering technique has been applied to overcome the eigenvalue identification problems. One of the most common clustering techniques is the K-mean clustering method which has been widely used for data grouping. However, the problem of local optima has become the main consideration in the K-mean clustering method [29]. To improve the K-mean clustering method, a spectral clustering algorithm is proposed. The N_{g}, Jordan, and Weiss (NJW) spectral clustering method is applied for clustering and identifying the trajectories and distribution of sensitive eigenvalues [30]. The procedure of the NJW is described as follows:

i. The affinity of matrix $\boldsymbol{A}$ or similarity between each pair of eigenvalue data x_i and x_j were calculated using this following equation:

$$\begin{aligned} A_{ij} &= \exp\left[\frac{\| x_i - x_j \|^2}{2\sigma^2}\right] \quad \text{for } i \neq j, \\ A_{ii} &= 0, \end{aligned} \tag{17}$$

where the scaling parameter of σ^2 constitutes the rate of affinity decrease with the distance between x_i and x_j.

ii. Construct the diagonal matrix of $\boldsymbol{D}$ using the sum of ith row of $\boldsymbol{A}$ as given by

$$D_{ii} = \sum_{j=1}^{n} A_{ij}. \tag{18}$$

iii. The Laplacian matrix of $\boldsymbol{L}$ can then be determined using the following equation:

$$\boldsymbol{L} = \boldsymbol{D}^{-1/2}\boldsymbol{A}\boldsymbol{D}^{-1/2}. \tag{19}$$

iv. Calculate the eigenvector and eigenvalues of $\boldsymbol{L}$.

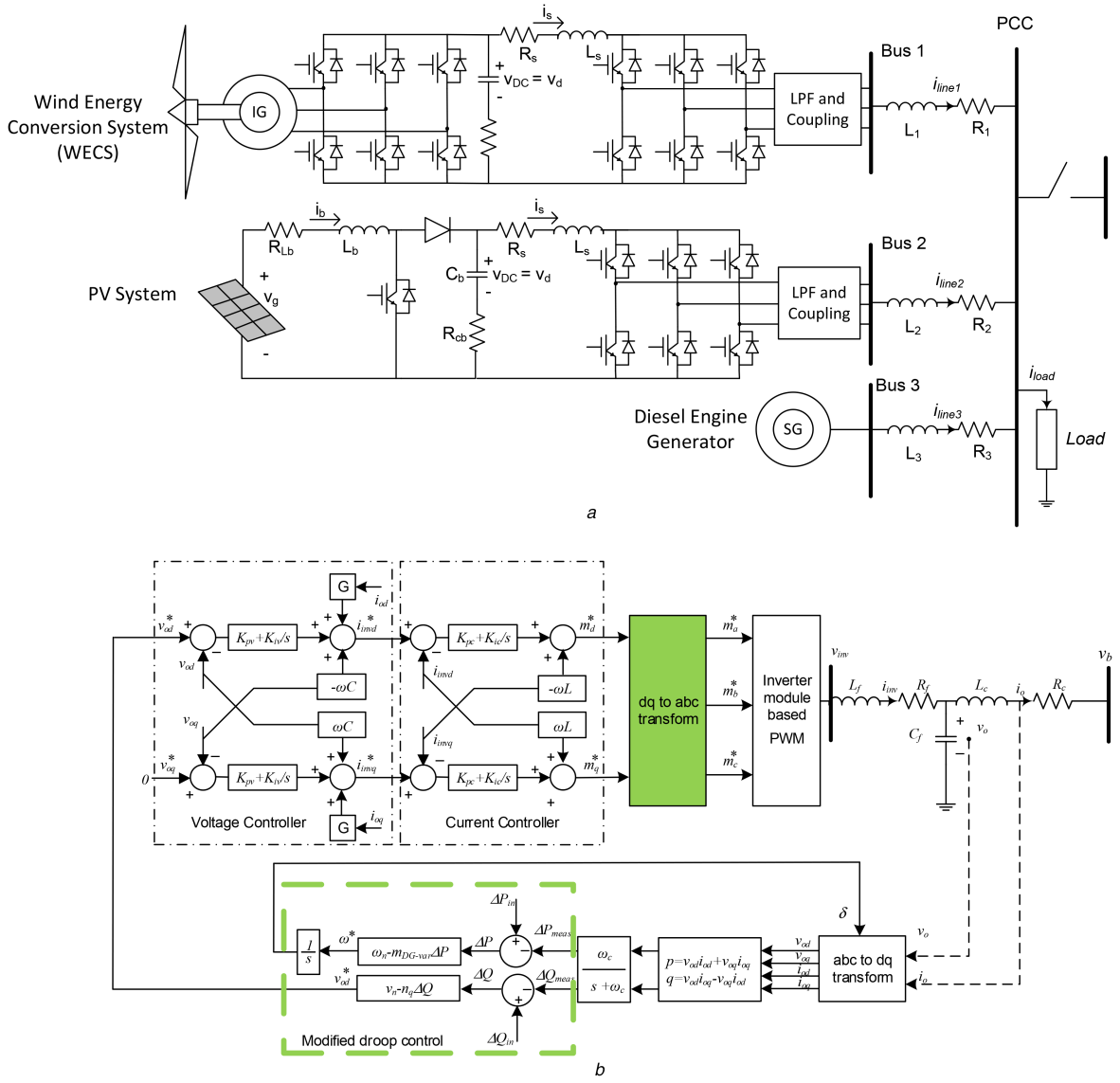

Fig. 1 *Investigated hybrid MG*
(a) Electrical circuit model,
(b) Grid side control with modified droop

v. Form a column matrix of $\boldsymbol{U}$ using the eigenvector of $\boldsymbol{L}$ corresponding to the k largest eigenvalues.
vi. Normalise the rows of $\boldsymbol{U}$ to form matrix $\boldsymbol{Y}$ in which the element of the corresponding matrix is determined as follows:

$$Y_{ij} = \frac{U_{ij}}{\sqrt{\sum_j U_{ij}^2}}. \tag{20}$$

vii Apply the K-means clustering to the rows of $\boldsymbol{Y}$.
.

The obtained eigenvalue cluster from the spectral K-Means clustering method is then observed through the participation factor analysis to make sure proper extraction of critical modes.

5 Hybrid MG model

Fig. 1 depicts the investigated hybrid MG system consisting of wind–PV and BDE [17] and the grid side inverter control of wind and PV-based DG units. Full converter WECS incorporates a back to back alternating current (AC)/direct current (DC)/AC converter as an interfacing device between a wind turbine and a local bus. While in a two-stage PV system, a boost DC/DC and DC/AC inverter system facilitated the connection between a solar PV array and a local bus. Mitigation of high-frequency distortion due to the inverter switching process is handled by the first-order low-pass filter. Moreover, the BDE is integrated into the hybrid MG to ensure load-generation balancing and provide synchronisation signal for other RES-based DG units.

Cascaded power electronic device architectures were considered in WECS and PV-based DG units. The control system associated with inverter-based DG units consisted of a generator and grid side controllers. In WECS, the flux-oriented control method is applied to enhance variable speed operation capability of the induction generator. While, in the photovoltaic (PV) system, the DC side input voltage control is realised by a conventional proportional-integral (PI) controller which regulated the difference between the optimum voltage from the maximum power point tracking (MPPT) controller and the measured DC link voltage. While the generator side controller ensures stable input for the RES-based DG unit, the grid side inverter control is responsible for providing regulation of active and reactive power output of DG units and maintaining stable output voltage.

A small signal model of the hybrid MG was analytically developed from the mathematical model of induction and synchronous machines, power electronic devices, and the associated controllers. A detailed modelling procedure of the investigated MG is presented in [17, 19]. A 62-order state matrix of the hybrid MG model consisting of voltage, current, output power and controller state variables from WECS (28 state variables), PV (18 state variables) and BDE (eight state variables) are considered in this study. Those state variables from each DG unit are then

combined with eight state variables of distribution lines and a central load to build a complete small signal model of the hybrid MG as shown in Fig. 1*a*.

Under the RES change, the generated power from the DG units changes accordingly, influencing the contribution of each DG unit in the power-sharing strategy. To manage with RES uncertainties, the existing droop gain control as presented in [17] should be modified. As RES varied, the droop gain controller is dynamically tuned to provide accurate power-sharing strategies in the hybrid MG. Moreover, since in the islanding operation, the MG should maintain the stability of local voltage and frequency, it is desirable that each DG unit also contributed to frequency and voltage regulations. The ancillary services of DG units in terms of local frequency and voltage supports are possible if there is sufficient power margin. Hence, to ensure adequate power is preserved for frequency regulation purpose, the WECS and PV might be operated slightly below its maximum operating point.

The modified grid side inverter control is presented in Fig. 1*b*. The proposed grid side controller consists of a modified power droop controller, outer voltage, and inner current controller loops. A power-sharing scheme in the MG is realised by the modified droop control method to take into account the availability of the RES according to its actual conditions. The modified droop control method is required to facilitate dynamic power sharing capability of the corresponded DG during RES fluctuation. Moreover, the reference values generated by modified droop control are used to generate a reference signal for an outer voltage control loop. Eventually, the output from the voltage control loop is applied to inner current control loops to generate a modulation signal for a DC/AC inverter.

Average active (ΔP_{meas}) and reactive (ΔQ_{meas}) power are determined by filtering the instantaneous active and reactive power as given by

$$\begin{aligned}\Delta P_{\text{meas}} &= \{\omega_{\text{c}}/(s+\omega_{\text{c}})\}\Delta p \rightarrow \text{d}\Delta P_{\text{meas}}/\text{d}t = \omega_{\text{c}}\Delta p - \omega_{\text{c}}\Delta P_{\text{meas}},\\ \Delta Q_{\text{meas}} &= \{\omega_{\text{c}}/(s+\omega_{\text{c}})\}\Delta q \rightarrow \text{d}\Delta Q_{\text{meas}}/\text{d}t = \omega_{\text{c}}\Delta q - \omega_{\text{c}}\Delta Q_{\text{meas}}.\end{aligned} \tag{21}$$

Modified droop control block generates frequency (ω*) and voltage (ω*) reference values for voltage controller loop. The reference values are determined as a function of droop parameter according to the following equations:

$$\begin{aligned}\omega^{*} &= \omega_{\text{n}} - m_{\text{DG-var}}(\Delta P_{\text{in}} - \Delta P_{\text{meas}}),\\ v_{\text{od}}^{*} &= v_{\text{n}} - n_{\text{q}}(\Delta Q_{\text{in}} - \Delta Q_{\text{meas}}),\end{aligned} \tag{22}$$

where ω_{n} and v_{n} represent the nominal values of frequency and voltage, respectively.

Active and reactive droop gain selections are conducted as a compromise between accurate power sharing, enhancement of dynamic response and voltage regulation. Since the MG small signal stability is less sensitive to reactive droop gain variation, only active droop gain variation from the RES based DG unit is considered in this study [14–16]. Reactive power droop gains in each DG are maintained constant throughout this work.

RES uncertainties regarding fluctuating conditions of solar irradiance and wind speed significantly influenced the power-sharing scheme among DGs. Droop gain values should be adjusted continuously to ensure accurate power sharing by RES variations. Moreover, during the islanding operation, each DG should contribute to maintain the system frequency. The frequency support from each DG is feasible if there is sufficient power margin. Hence, to ensure adequate power preserve for a frequency regulation purpose, the WECS and PVs might be operated slightly below its maximum operating point. A proposed dynamic droop parameter considering RES variation and power preserve for the frequency regulation purpose is given by

$$m_{\text{DG-var}} = \left(m_{\max} - (m_{\max} - m_{\min})\left\{\frac{P_{\text{input}}}{P_{\max}}\right\}\right), \tag{23}$$

where P_{input} and $P_{\max}$ represent actual input power from RES and maximum power of DGs, respectively. The active droop gain control is regulated within the specified maximum ($m_{\max}$) and minimum ($m_{\min}$) limit.

For PV-based DG, the droop gain can be calculated by substituting (7) into (23) as given by the following equation:

$$\begin{aligned}m_{\text{PV-var}} &= m_{\max} - (m_{\max} - m_{\min})\frac{V_{\text{pv}}N_{\text{p}}}{P_{\max}}\\ &\left\{I_{\text{sc}}\left(\frac{G_0}{G_{\text{ref}}}\right) - I_{\text{s}}\text{e}^{(qV_{\text{pv}}/nkTN_{\text{s}})}\right\},\end{aligned} \tag{24}$$

where G_0 represents the initial condition of solar irradiance around a certain operating point.

The grid side DC/AC inverter control in WECS adopted a similar modified droop controller method as in the PV system. Active droop gain control considering wind speed variation is determined by substituting (1) into (23) as given by

$$m_{\text{WECS-var}} = m_{\max} - (m_{\max} - m_{\min})\left\{\frac{0.5\rho C_{\text{opt}}(\lambda_{\text{opt}}, \beta)A_{\text{r}}v_{\text{w0}}^{3}}{P_{\max}}\right\}, \tag{25}$$

where v_{w0} represents an initial condition of wind speed around a certain operating point. It is assumed that power input from a certain wind speed is a function of a given wind speed with a constant tip speed ratio and blade pitch angle.

The modified droop control method is then incorporated into the state space model of WECS and PV, as in [17] to develop a comprehensive hybrid MG model considering wind speed and solar irradiance uncertainties.

6 Results and discussions

A complete model of the hybrid MG system consisting of PV, WECS, and BDE was developed by adapting parameters of WECS and BDE from [31–33]. The small signal model of 3 MVA capacity of each WECS, photovoltaic (PV), and BDE (bio diesel engine) generator was combined with a state space model of the network impedance to supply an aggregated 5 MW central load. Modal analysis was focused on critical eigenvalues which significantly influenced stable operations of the hybrid MG. The dynamic behaviour of the hybrid MG in autonomous operation is investigated by considering uncertainties of wind speed and solar irradiance. The distribution of critical eigenvalues corresponding to the damping ratio and oscillatory frequency is then thoroughly observed to assess the system dynamic performance and risk of instability events.

6.1 Wind speed estimations

Annual wind speed data from four wind stations with hourly sampling resolution were considered. The Weibull distribution function was fitted to the historical wind speed data. Shape (k) and scale (c) parameters of the Weibull function for wind speed in regions 1–4 (WR1 to WR4) were determined using the maximum likely method as listed in Table 1. The obtained Weibull parameters were then utilised for estimating the PDFs of the wind speed as depicted in Fig. 2*a*. From the estimated PDFs, 10,000 wind speed data were generated and randomly sampled through MCS to realise the practical scenarios of wind uncertainties.

Statistical analysis corresponding to the mean and standard deviation of the actual and estimated wind velocity distribution is shown in Table 2. It was suggested that <5% difference between mean and standard deviation between real and estimated wind speed data was observed. Hence it can be considered that the Weibull distribution function was feasible to estimate the wind

Table 1 Parameters of wind speed Weibull PDF

Parameters	WR1	WR2	WR3	WR4
scale (c)	5.602	6.031	5.673	7.911
shape (k)	1.721	1.811	1.607	1.514

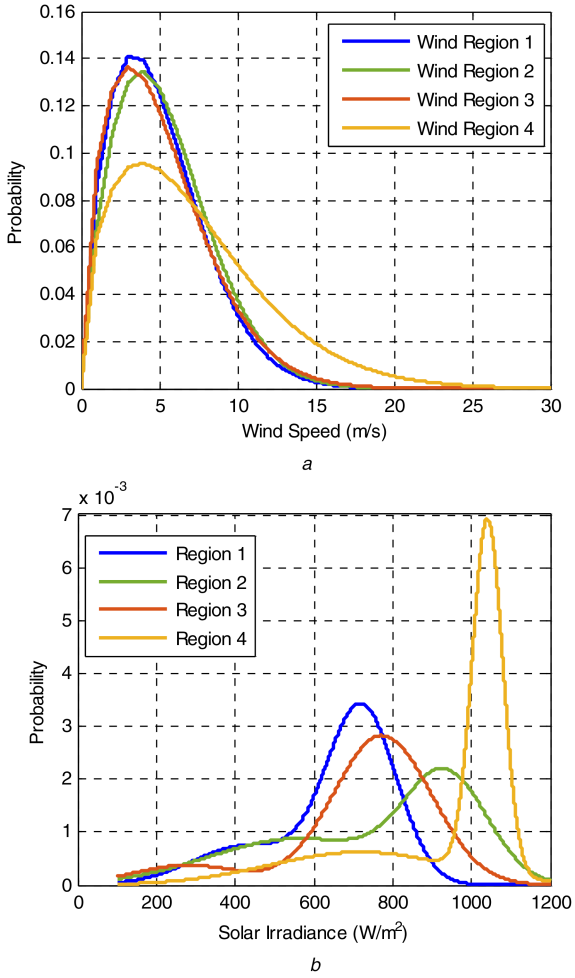

Fig. 2 *Estimated PDF of RES in four regions*
(a) Wind speed PDFs,
(b) Solar irradiance PDFs

speed PDFs. The more fluctuating condition of wind speed was characterised by higher mean and deviation of the wind speed PDFs.

6.2 Solar irradiance estimations

A similar estimation procedure has been followed for determining solar irradiance distribution. Annual data of solar irradiance from four different locations are considered. From the hourly data, the parameters of the mixture Gaussian PDF function were calculated, and thus the PDFs for hourly solar irradiance can be determined. In this study, the distribution of solar irradiance during mid-day time in four different regions was considered. The estimated parameters of the mixture Gaussian distribution functions of solar irradiance data are listed in Table 3. From the estimated parameters of the mixture Gaussian function, solar irradiance distribution can be determined as presented in Fig. 2*b*. From the obtained mixture Gaussian distribution function parameters, the solar irradiance PDFs can be estimated for MCS purpose. In this study, 10,000 random samples of solar irradiance were generated to realise the practical scenario of solar irradiance variation.

Statistical analysis corresponding to the mean and standard deviation of the actual and estimated irradiance distribution is shown in Table 4. It was suggested that <10% difference between mean and standard deviations of actual and estimated irradiance data was observed. Hence, it can be considered that the mixture Gaussian distribution function was feasible for estimating the solar irradiance PDFs.

6.3 Probabilistic small signal stability of hybrid MG considering uncertainties

The generated random values of wind speed and solar irradiance were applied to the hybrid MG to investigate system dynamic behaviour and small signal stability performance. Combinations of wind speed and solar f irradiance PDFs from four selected regions were considered. It is assumed that under islanding operation, all DG units in the MG contributed to the power-sharing scheme to supply the load demand and power from WECS and PV dominantly contributed in power-sharing strategies of the investigated hybrid MG. While BDE contributed to overcoming the shortfall of power from the two RES-based DG units.

Table 2 Statistical analysis of Weibull PDF for wind speed estimations

Wind regime	Mean		Err., %	St. deviation		Err., %
	Act.	Est.		Act.	Est.	
WR1	5.361	5.414	0.985	3.048	3.007	1.359
WR2	5.756	5.803	0.816	3.103	3.087	0.522
WR3	5.427	5.502	1.389	3.323	3.250	2.191
WR4	7.501	7.599	1.311	5.045	4.966	1.573

Table 3 Parameters of mixture Gaussian PDF for solar irradiance estimation

Solar reg.	Parameters					
	Weight (τ_1)	Mean (μ_1)	Std. (σ_1)	Weight (τ_2)	Mean (μ_2)	Std. (σ_2)
SR1	0.259	432.67	138.92	0.741	720.99	88.51
SR2	0.127	280.53	136.02	0.873	774.01	124.75
SR3	0.494	561.09	228.05	0.506	935.99	104.04
SR4	0.359	721.23	231.50	0.641	1041.3	38.52

Table 4 Statistical analysis of solar irradiance

Solar reg.	Mean		Err., %	St. dev.		Err., %
	Act.	Est.		Act.	Est.	
SR1	718.04	746.92	4.023	198.47	192.47	3.023
SR2	651.56	648.89	0.410	175.50	182.97	4.084
SR3	750.91	803.42	6.994	240.46	231.48	3.881
SR4	926.28	886.74	4.269	209.24	219.42	4.867

Table 5 Investigated modes from WECS and PV-based DG units

Critical modes	Complex values	F, Hz	ζ, %	Participation factor
$\lambda_{42,43}$	−0.617 ± 7.024	1.118	8.751	P_{WECS}, Q_{WECS},P_{PV}, Q_{PV}
$\lambda_{45,46}$	−1.544 ± 10.799	1.716	14.153	P_{PV}, Q_{PV},P_{WECS}, Q_{WECS},

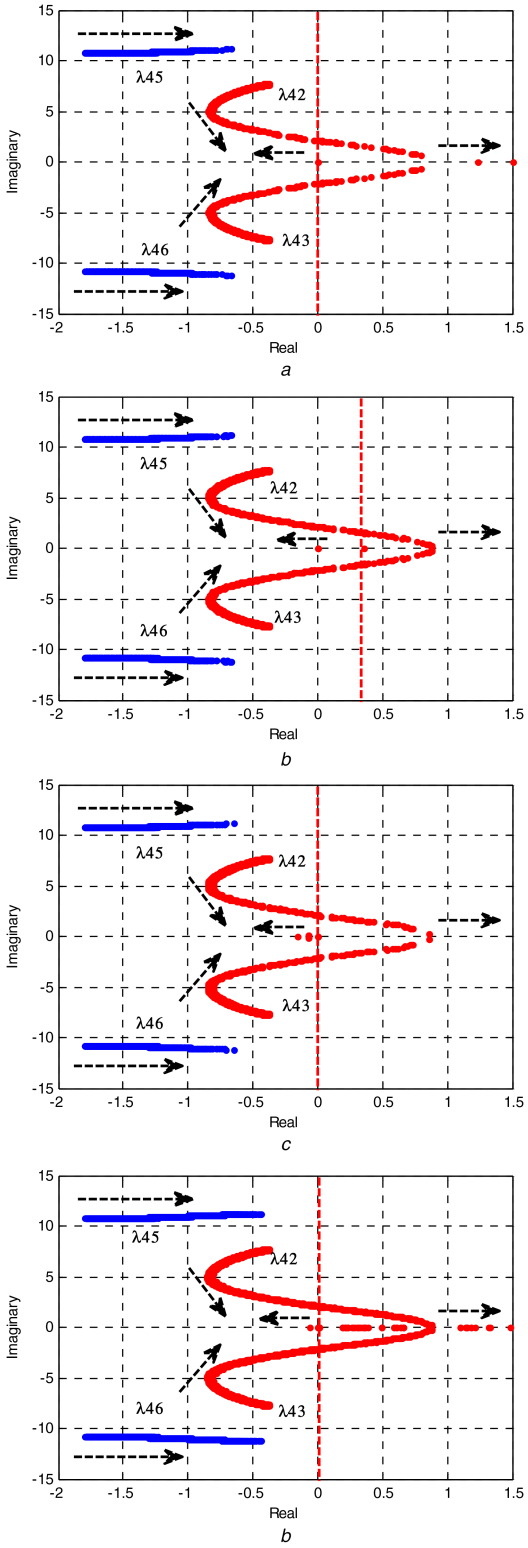

Fig. 3 *Trajectories of sensitive modes under wind speed and solar irradiance uncertainties in*
(a) Region 1,
(b) Region 2,
(c) Region 3,
(d) Region 4

The power output of RES-based DG units in the MG strongly correlated with the availability of RES and setting of a droop gain controller. Under fluctuated conditions of wind speed and solar irradiance, the power-sharing scheme among WECS and PV should be updated continuously. In this study, a maximum and minimum active power droop setting were set at 8 and 4%, respectively. The droop gain might be varied within the specified limit in accordance with RES variation. The change of the power-sharing strategy significantly influenced the MG dynamic response. The non-linear dynamic behaviour of the critical eigenvalues corresponding to power output from the RES-based DGs should be monitored to evaluate the risk of instability. Critical eigenvalues related to DG power output and droop control scheme were characterised by a low-frequency oscillation. It was also monitored that the WECS and PV were not fully decoupled due to the presence of highly resistive lines [14]. A connection between those DG units was confirmed by participation factor analysis which monitored the contribution of particular state variables in the modes. It was suggested that active power, phase angle and reactive power state variables from WECS and PV were participating in modes of $\lambda_{42,43}$ and $\lambda_{45,46}$ as listed in Table 5. Even though the damping ratio of the investigated modes was above the critical situation (>5%) in a base case scenario with 8 m/s wind speed and 1000 W/m^2 solar irradiance, the corresponding modes were susceptible to wind speed and solar irradiance variations and potentially caused instability to the hybrid MG.

MCS with the RES uncertainties is applied to the hybrid MG system. The 10,000 random values of wind speed and solar irradiance from four different regions were generated to realise the practical scenario of islanding MG operation. Under RES changes, the sensitive eigenvalues corresponding to power output from the DG behaved randomly which is reflected in the non-linear and uncertain eigen-trajectories. Participation factor analysis and spectral K-mean clustering methods were combined to identify the critical eigenvalues. The obtained eigen-cluster related to the critical eigenvalues from regions 1–4 are depicted in Fig. 3. As solar irradiance varied, the small signal stability of the hybrid MG was affected considerably. The more oscillatory condition was monitored with the increase of solar irradiance, indicated by the right movement of eigenvalues of $\lambda_{45,46}$. System damping deteriorated severely when wind speed fluctuated. The oscillatory frequency of WECS modes significantly decreased from 1.21 to 0.47 Hz as wind speed continuously varied. At higher wind speed, the hybrid MG becomes unstable. The unstable conditions were visualised by an extensive departure of eigenvalues of $\lambda_{42,43}$ across the imaginary axis to the right half complex plane.

The distribution of investigated modes from WECS and PV under uncertain RES conditions is presented in Tables 6 and 7, respectively. The deviation of the real part, imaginary part and damping ratio of critical modes correlated to eigenvalues dynamic behaviour under RES change. Higher deviation of imaginary part of eigenvalues $\lambda_{42,43}$ than $\lambda_{45,46}$ was monitored. This result indicated that the frequency of oscillation of WECS was more affected by fluctuating condition of wind speed, while the oscillatory state of PV-based DGs was less influenced by an irradiance change. It was also observed that the damping ratio of the modes associated with WECS was significantly affected by RES variations. The extensive movement towards the right half complex plane and higher deviation on system damping of critical modes from WECS indicated deterioration of small signal stability. Therefore, a possible unstable event in islanding operation of hybrid MG might happen under high wind speed circumstances.

The assessment of small signal stability performance was conducted by evaluating the distribution of critical modes damping ratio. Figs. 4–7 show the trajectories of critical modes and their associated damping ratio distributions. It was monitored that in

Table 6 Statistical analysis of critical modes from WECS

Reg.	Eigenvalues of $\lambda_{42,43}$					
	Re.		Im.		Damping, %	
	Mean	Std.	Mean	Std.	Mean	Std.
reg. 1	−0.484	0.139	7.199	1.047	6.585	9.488
reg. 2	−0.498	0.135	7.214	0.902	6.941	6.923
reg. 3	−0.485	0.132	7.267	0.849	6.719	6.732
reg. 4	−0.475	0.325	6.402	2.119	6.088	26.531

Table 7 Statistical analysis of critical modes from PV

Reg.	Eigenvalues of $\lambda_{45,46}$					
	Re.		Im.		Damping, %	
	Mean	Std.	Mean	Std.	Mean	Std.
reg. 1	−1.652	0.168	10.791	0.041	15.134	1.547
reg. 2	−1.646	0.156	10.793	0.035	15.081	1.439
reg. 3	−1.663	0.149	10.784	0.033	15.236	1.376
reg. 4	−1.525	0.282	10.831	0.089	13.955	2.614

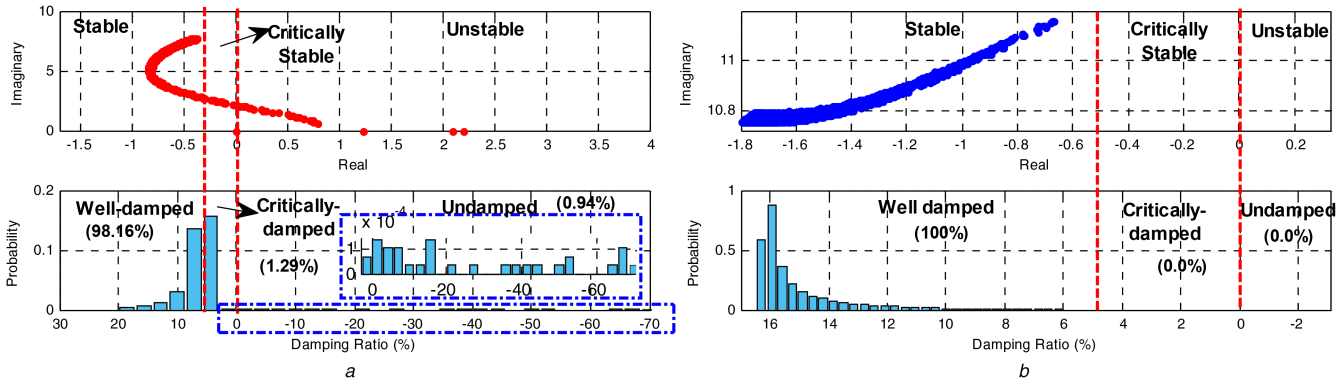

Fig. 4 *Stability assessment of critical modes from*
(a) *WECS,*
(b) PV-based DGs in region 1

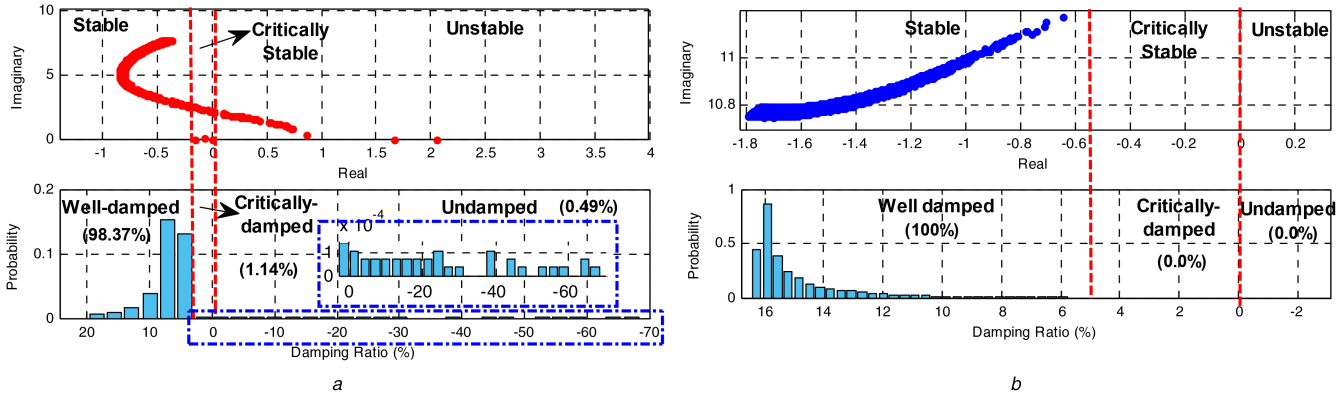

Fig. 5 *Stability assessment of critical modes from*
(a) *WECS,*
(b) PV-based DGs in region 2

regions 1–3, eigenvalues from the PV-based DG was stable under RES uncertainties. A 100% well-damped dynamic response, characterised by $\zeta \geq 5\%$, was observed. As more fluctuating wind speed was experienced in region 4, the stability margin of PV modes slightly decreased. It was monitored that the probability of critically stable situation was 0.43%. Small disturbance risk assessment was then applied to critical modes from WECS. The stability margin of the corresponding modes can be maintained above 95% in all four regions. The occurrence of the critical situation was observed under 2% while the risk of unstable events was monitored under 6%. The highest risk of instability of 5.44% was identified in the region four which had the highest wind speed fluctuation.

The MG is required to deal with all possible power-sharing strategies corresponding to the variation of the RES. Therefore, the power-sharing scheme should be dynamically adjusted to ensure balance condition between power generation and demand. The purpose of this work is to investigate the dynamic performance of the MG under dominant supplies from RES-based DG units such as wind and PV. Therefore, it is considered that the BDE is operated <20% of its capacity. While 80% power demand is handled proportionally by WECS and PV-based DG units according to the dynamic setting of the power droop controller which varied according to the actual RES conditions.

Fig. 8 shows the time domain simulation of the system dynamic response of each DG when the MG in region four was operated

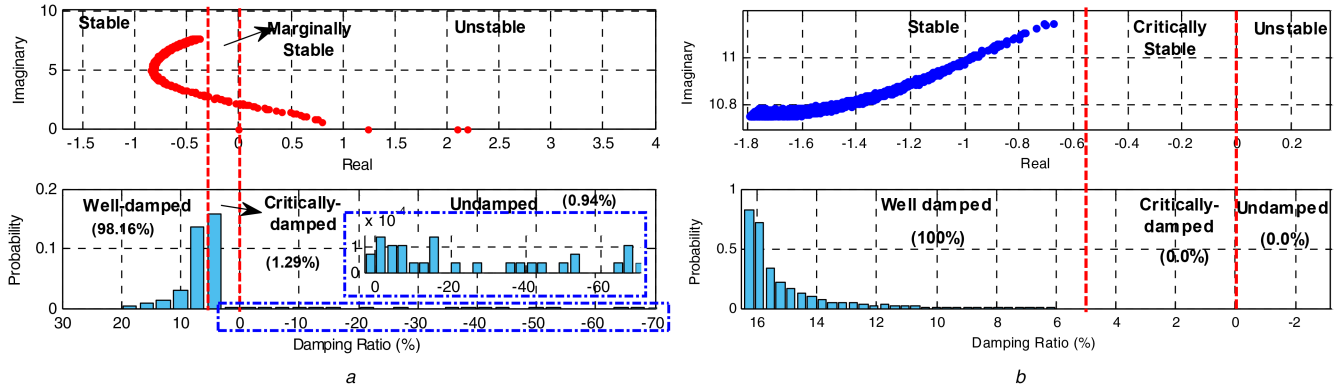

Fig. 6 *Stability assessment of critical modes from*
(a) *WECS,*
(b) PV-based DGs in region 3

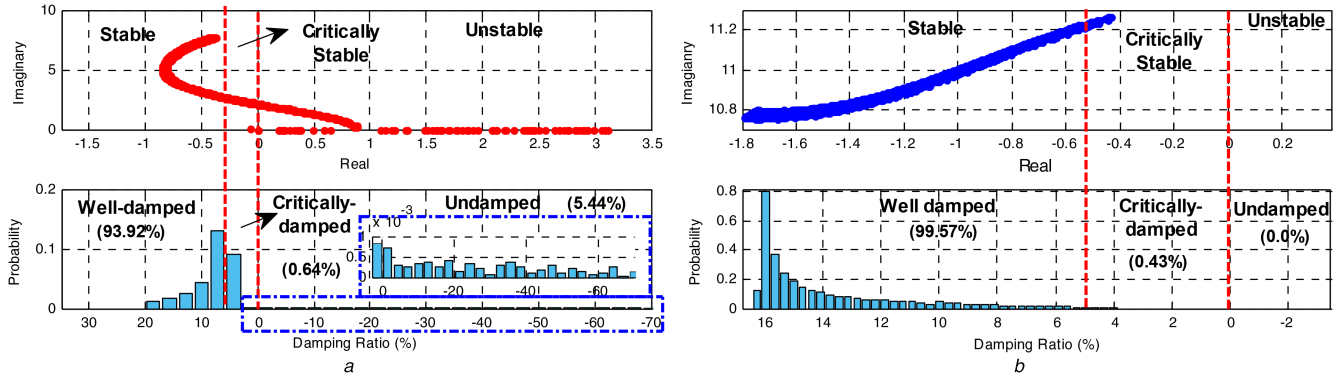

Fig. 7 *Stability assessment of critical modes from*
(a) *WECS,*
(b) PV-based DGs in region 4

under wind speed fluctuations. In the first scenario, it was considered that initially the MG was operated at 10 m/s wind speed and 1000 W/m^2 solar irradiance. Small step changes of wind speed from 10 to 11 m/s and from 11 to 10.5 m/s occurred at 99 and 130 s, respectively. The second scenario considered the operation of the hybrid MG at higher wind speed condition of 13 m/s and constant solar irradiance of 1000 W/m^2. A small perturbation of wind velocity from 13 to 14 m/s and from 14 to 13.5 m/s occurred at 99 and 130 s, respectively.

The contribution of WECS, PV, and BDE in the power-sharing scheme in first and second scenarios is presented in Fig. 8*a* and *b*, respectively. As wind speed fluctuated, the power contribution from WECS varied proportionally. The change of wind speed affected the power-sharing strategy among RES-based DGs. Even though the solar irradiance was assumed constant in both scenarios, the power contribution of the PV-based DG unit slightly changed as wind speed fluctuated since those two DG units were not fully decoupled. Hence the variation in the DG unit would affect the other DG unit. Moreover, dynamic droop control action also influences the output power from each DG unit to maintain generator-load balance in the MG. While power contribution from the BDE was relatively constant since it was considered as a reference DG unit to ensure synchronisation among the DG units and provide additional power to overcome the shortfall energy from WECS and PV. It was monitored that when the MG was operated at higher wind speed, deterioration of oscillatory stability conditions occurred, indicated by more oscillatory of the dynamic response as shown in Fig. 8*b*. The MG small signal stability performance improved when the hybrid MG was operated under lower wind speed situation as shown in Fig. 8*a*. The system dynamic response was enhanced, indicated by the less oscillatory condition. Moreover, it was considered that BDE-based DG unit was operated as a reference DG. Hence, the contribution of the BDE was relatively similar in both scenarios. The obtained results from the time domain simulation were consistent with the previous probabilistic modal analysis presented in Figs. 4–7.

7 Conclusions

Probabilistic small signal stability analysis considering RES uncertainties in islanding operation of a hybrid MG is presented in this study. The uncertain conditions of wind speed and solar irradiance from four different regions were applied to the developed hybrid MG model consisting of WECS, PV, and BDE-based DG units. The trajectories and distribution of critical modes damping ratio and frequency of oscillation were thoroughly investigated through MCS. From the probabilistic study, it was suggested that the presence of wind speed and solar irradiance uncertainties resulted in a dynamic change of power-sharing strategies among DGs in the MG. Moreover, it had an adverse effect on small signal stability, in particular to low-frequency critical modes of the MG. It was also observed that the uncertain condition of wind speed introduced more deterioration in system damping than solar irradiation variation, indicated by the extensive movement of the critical eigenvalues toward the imaginary axis. When the MG was operated at higher wind speed condition, less system damping was observed indicated by more oscillatory of the dynamic response. The obtained time domain simulation results confirmed the probabilistic eigenvalue analysis.

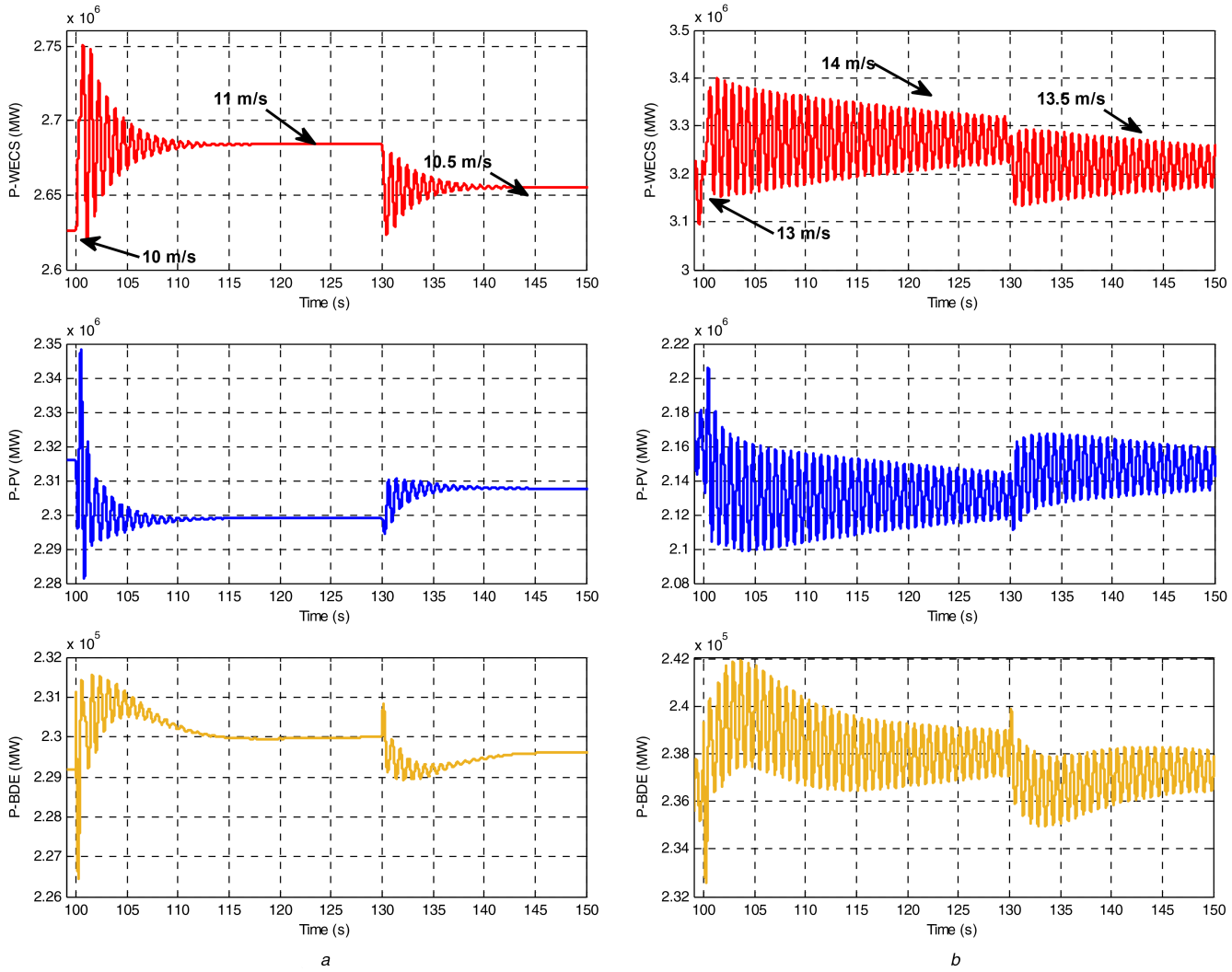

Fig. 8 *Power-sharing scheme of WECS, PV, and BDE in*
(a) First scenario,
(b) Second scenario

8 References

[1] Rueda, J.L., Colomé, D.G., Erlich, I.: 'Assessment and enhancement of small signal stability considering uncertainties', *IEEE Trans. Power Syst.*, 2009, **24**, pp. 198–207

[2] Ahmadi, H., Seifi, H.: 'Probabilistic tuning of power system stabilizers considering the wind farm generation uncertainty', *Electr. Power Energy Syst.*, 2014, **63**, pp. 565–576

[3] Shi, L.B., Wang, C., Yao, L.Z., *et al.*: 'Analysis of impact of grid-connected wind power on small signal stability', *Wind Energy*, 2011, **14**, pp. 517–537

[4] Rueda, J.L., Colome, D.G.: 'Probabilistic performance indexes for small signal stability enhancement in weak wind-hydro-thermal power systems', *IET Gener. Transm. Distrib.*, 2009, **3**, pp. 733–747

[5] Bu, S.Q., Du, W., Wang, H.F., *et al.*: 'Probabilistic analysis of small-signal stability of large-scale power systems as affected by penetration of wind generation', *IEEE Trans. Power Syst.*, 2012, **30**, pp. 2479–2486

[6] Rueda, J.L., Erlich, I.: 'Probabilistic framework for risk analysis of power system small-signal stability', *Proc. Inst. Mech. Eng. O, J. Risk Rel.*, 2012, **1**, pp. 118–133

[7] Yue, H., Li, G., Zhou, M.: 'A probabilistic approach to small signal stability analysis of power systems with correlated wind sources', *J. Electr. Eng. Technol.*, 2013, **8**, pp. 742–751

[8] Milanović, J.V.: 'Probabilistic stability analysis: the way forward for stability analysis of sustainable power systems', *Phil. Trans. R. Soc. A*, 2017, **375**, pii: 20160296, pp. 1–22.

[9] a, G.L., Yuea, H., Zhoua, M., *et al.*: 'Probabilistic assessment of oscillatory stability margin of power systems incorporating wind farms', *Electr. Power Energy Syst.*, 2014, **58**, pp. 47–56

[10] Ayodele, T.R.: 'Analysis of Monte Carlo simulation sampling techniques on small signal stability of wind generator-connected power system', *J. Eng. Sci. Technol.*, 2016, **11**, (4), pp. 563–583

[11] Bian, X.Y., Geng, Y., Lo, K.L., *et al.*: 'Coordination of PSSs and SVC damping controller to improve probabilistic small-signal stability of power system with wind farm integration', *IEEE Trans. Power Syst.*, 2016, **31**, pp. 2371–2382

[12] Xu, X., Lin, T., Zha, X.: 'Probabilistic analysis of small signal stability of microgrid using point estimate method'. Int. Conf. on Sustainable Power Generation and Supply, 2009 (SUPERGEN'09), 2009

[13] Elizondo, J., Zhang, R.Y., White, J.K., *et al.*: 'Robust small signal stability for microgrids under uncertainty'. 2015 IEEE 6th Int. Symp. on the Power Electronics for Distributed Generation Systems (PEDG), Aachen, 2015

[14] Pogaku, N., Prodanovic, M., Green, T.C.: 'Modeling, analysis and testing of autonomous operation of an inverter-based microgrid', *IEEE Trans. Power Electron.*, 2007, **22**, pp. 613–625

[15] Barklund, E., Pogaku, N., Prodanovic, M., *et al.*: 'Energy management in autonomous microgrid using stability-constrained droop control of inverters', *IEEE Trans. Power Electron.*, 2008, **23**, pp. 2346–2351

[16] Mohamed, Y.A.-R.I., El-Saadany, E.F.: 'Adaptive decentralized droop controller to preserve power sharing stability of paralleled inverters in distributed generationmicrogrids', *IEEE Trans. Power Electron.*, 2008, **23**, pp. 2806–2816

[17] Krismanto, A.U., Nadarajah, M.: 'Identification of modal interaction and small signal stability in autonomous microgrid operation', *IET Gen. Transm. Distrib.*, 2017, http://dx.doi.org/10.1049/iet-gtd.2017.1219, early access

[18] Bottrell, N., Prodanovic, M., Green, T.C.: 'Dynamic stability of a microgrid with an active load', *IEEE Trans. Power Electron.*, 2013, **28**, pp. 5107–5119

[19] Krismanto, A.U., Mithulananthan, N., Lee, K.Y.: 'Comprehensive modeling and small signal stability analysis of RES-based microgrid'. 9th IFAC Symp. on Control of Power and Energy Systems (CPES) New Delhi, 2015

[20] Shahabi, M., Haghifam, M.R., Mohamadian, M., *et al.*: 'Microgrid dynamic performance improvement using a doubly fed induction wind generator', *IEEE Trans. Energy Convers.*, 2009, **24**, pp. 137–145

[21] Rocha, P.A.C., Sousa, R.C.D., de Andrade, C.F., *et al.*: 'Comparison of seven numerical methods for determining Weibull parameters for wind energy generation in the northeast region of Brazil', *Appl. Energy*, 2012, **89**, pp. 395–400

[22] Werapuna, W., Tirawanichakul, Y., Waewsakc, J.: 'Comparative study of five methods to estimate Weibull parameters for wind speed on Phangan island, Thailand'. 2015 Int. Conf. on Alternative Energy in Developing Countries and Emerging Economies, 2015

[23] Tan, Y.T., Kirschen, D.S., Jenkins, N.: 'A model of PV generation sui for stability analysis', *IEEE Trans. Energy Convers.*, 2004, **19**, pp. 748–755
[24] Tina, G., Gagliano, S.: 'Probability analysis of weather data for energy assessment of hybrid solar/wind power system'. 4th IASME/WSEAS Int. Conf. on Energy, Environment, Ecosystems and Sustainable Development (EEESD'08), Algarve, Portugal, 2008
[25] Atwa, Y.M.: 'Distribution system planning and reliability assessment under high DG penetration'. PhD, Electrical and Computer Engineering, University of Waterloo, Ontario, Canada, 2010
[26] Jurado, M., Caridad, J.M., Ruiz, V.: 'Statistical distribution of the clearness index with radiation data integrated over five minutes interval', *Sol. Energy*, 1995, **5**, pp. 469–473
[27] Lee, I.E., Sim, M.L., Kung, F.W.L., *et al.*: 'Statistical analysis and modelling of one-minute global solar irradiance for a tropical country'. 2nd Int. Symp. on Environment-Friendly Energies and Applications (EFEA), 2012
[28] Kundur, P., Balu, N.J., Lauby, M.G.: '*Power system stability and control*' (McGraw-Hill, New York, NY, USA, 1994)
[29] Verma, D., Meila, M.: 'A comparison of spectral clustering algorithms'. Technical Report UW-CSE-03-05-01, University of Washington, 2003
[30] Martinez, W.L., Martinez, A.R., Solka, J.L.: '*Exploratory data analysis with MATLAB®*' (Taylor & Francis Group, London, 2011, 2nd edn.)
[31] Krause, P.C., Wasynczuk, O., Sudhoff, S.D.: '*Analysis of electric machinery and drive system*' (Wiley-Interscience, New York, 2002, 2nd edn.)
[32] Wu, B., Lang, S.D., Zargari, N., *et al.*: '*Power conversion and control of wind energy systems*' (John Wiley & Sons, Inc,, New Jersey, 2011)
[33] Ugalde-Loo, C.E., Ekanayake, J.B., Jenkins, N.: 'State-space modeling of wind turbine generators for power system studies', *IEEE Trans. Ind. Appl.*, 2013, **48**, pp. 223–232

9 Appendix

See Table 8.

Table 8 System parameters

Parameter	Symbol	Value
rated voltage	V_{base}	690 V
parasitic resistance of DC/DC inductor	R_b	1 mΩ
DC/DC inductor	L_b	2 mH
parasitic resistance of DC/DC capacitor	R_{cb}	1 mΩ
DC/DC capacitor	C_b	1000 μF
AC input side Inductance of AC/DC	L_{sw}	1 mH
AC input side capacitor of AC/DC	C_{inw}	1000 μF
AC side resistance of AC/DC converter	R_{sdcw}	10 mΩ
DC side capacitor of DC/AC converter	C_{coutw}	1000 μF
DC side inductance of DC/AC inverter	L_{sdcw}	6.43 mH
DC link inductance	L_{link}	0.01 mH
DC link resistance	R_{link}	1 mΩ
DC link capacitance	C_d	6500 μF
low pass filter inductance	L_f	1 mH
low pass filter capacitance	C_f	100 μF
low pass filter resistance	R_f	1 mΩ
coupling inductance	L_c	0.1 mH
coupling resistance	R_c	1 mΩ
load resistance	R_{lo}	0.95 Ω
load inductance	L_{lo}	10 mH
line resistance (buses 1, 2 and 3)	R_{li}	10 mΩ